Optical Bend Sensor Based on Eccentrically Micro-Structured Multimode Polymer Optical Fibers

Lennart Leffers, Julia Locmelis, Kort Bremer, Bernhard Roth, and Ludger Overmeyer

***Abstract*—We report on a novel bend sensor with high flexibility and elasticity based on Bragg grating structures in polymer optical fibers to detect bending for the measurement of movement. The concept is very simple and relies on the inscription of eccentrical Bragg gratings into multimode graded-index polymer optical fibers via contact exposure with a krypton fluoride excimer laser in the ultraviolet region and an optimized phase mask. Depending on the fiber deformation, the lattice constant of the inscribed Bragg grating is strained or compressed due to its position relative to the fiber core. This in turn results in a specific shift of the Bragg wavelength of up to 1.3 nm to the red or blue wavelength region, respectively, which is sufficiently large to be reliably detected. Therefore, as proof of principle, deformation along one axis can be observed with a single Bragg grating with a maximum sensitivity of up to 65 pm/m^{-1}. Moreover, multiple Bragg gratings inscribed into the same polymer optical fiber at different positions around the fiber axis allow to determine the shape deformation of the fiber relative to a reference frame with similar accuracy. Consequently, this technology could form the basis for new applications in the areas of medical diagnostics, robotics or augmented reality, which are lacking affordable sensor systems to date.**

***Index Terms*—Fiber Bragg gratings, fiber optics, optical bend sensor, polymer optical fiber, UV excimer laser.**

I. Introduction

IN RECENT years polymer optical fibers with inscribed fiber Bragg gratings (FBG) have emerged as potential sensors for various purposes such as strain, temperature, humidity, pressure, vibration or bending [1]–[7]. Compared to silica glass fibers, polymer optical fibers (POF) have several advantages such as a lower Young's modulus, higher flexibility, higher elastic strain and ductile breaking limits while they are still inhibiting the critical benefits of silica glass fibers compared to metallic electrical conductors [7], [8]. Since the first reported inscription of FBGs in POF in 1999 [9], different kinds of fibers, such as single-mode, multimode and micro-structured fibers were employed for FBG fabrication [9]–[12]. As fiber materials often Polymethylmetacrylate (PMMA) is used, since its material characteristics are well known and PMMA fibers are widely available [10]–[12]. Also cyclic transparent optical polymer (CYTOP) is emerging as fiber material [13], since it offers some advantages over, e.g., PMMA such as high chemical stability and low attenuation in the infrared region [8], which renders it suitable to even replace silica glass fibers in common applications. As methods for inscription of a Bragg grating (BG) into POF either Ultraviolet-exposure (UV) with phase masks [7], [12], [13] or direct-write methods with femtosecond lasers are known [14]–[17]. Femtosecond lasers can alter the material at precise positions by plane-by-plane or point-by-point methods, which usually leads to strong gratings with 90 percent reflection efficiency. On the other hand the phase mask method is more simple but alters the material only from the surface onwards into the bulk, where the depth also relates to the reflectivity of the gratings.

Additionally to the usual applications of POF to sense changes in strain, temperature, humidity or pressure, for example in structural health monitoring [18], [19], we here present an FBG sensor to detect bending precisely at one spot. Beforehand, this was performed with uneven or asymmetric fibers [2], [5], [20], multiple fibers [21], multi-core fibers [2], [22]–[25] or additional optical elements [26]. The new sensor concept presented in this work employs a single multimode fiber and a single FBG for sensing of angular movement in one direction or multiple FBGs at the same position along the optical axis of the fiber (FBG triplets) for sensing of angular movement in 3D (Fig. 1). Apart from the simplicity of the concept itself its manufacturing is also very simple, i.e. the inscription of the FBGs, the connection to an interrogation system and ultimately also the production of the polymer fibers, which is an overall benefit with regard to production time and cost. Compared to that, other approaches require more complex processes for example for the production of fibers [2], [5], [20], [22], the focusing of the laser light on single fiber cores of the multi-core fibers during inscription [2], [23], [25] or the connection to the measurement system based on fiber splicing [22] or fan-outs [24]. We report on production and detection of the eccentric BG under the surface of the graded-index core of a CYTOP fiber and validate the sensitivity for detection of bending in a proof-of-principle experiment. The realized bend sensor is expected to find applications in various kinds of 2D or 3D movement control scenarios.

Manuscript received June 10, 2021; revised August 27, 2021; accepted September 6, 2021. Date of publication September 9, 2021; date of current version September 28, 2021. This work was supported in part by the Deutsche Forschungsgemeinschaft (DFG, German Research Foundation (OV 36/43-1)). The work of Kort Bremer, Bernhard Roth and Ludger Overmeyer was supported in part by the Deutsche Forschungsgemeinschaft (DFG, German Research Foundation) under Germany's Excellence Strategy within the Cluster of Excellence PhoenixD (EXC 2122, Project ID 390833453). *(Corresponding author: Lennart Leffers.)*

Lennart Leffers and Julia Locmelis are with the Hannover Centre for Optical Technologies, Gottfried Wilhelm Leibniz University Hanover, 30167 Hannover, Germany (e-mail: lennart.leffers@hot.uni-hannover.de; julia-locmelis@htp-tel.de).

Kort Bremer and Bernhard Roth are with the Hannover Centre for Optical Technologies, Gottfried Wilhelm Leibniz University Hanover, 30167 Hannover, Germany, and also with the Cluster of Excellence PhoenixD, 30167 Hannover, Germany (e-mail: kort.bremer@hot.uni-hannover.de; bernhard.roth@hot.uni-hannover.de).

Ludger Overmeyer is with the Hannover Centre for Optical Technologies, Gottfried Wilhelm Leibniz University Hanover, 30167 Hannover, Germany, with the Cluster of Excellence PhoenixD, 30167 Hannover, Germany, and also with the Institute of Transport and Automation Technology, Gottfried Wilhelm Leibniz University Hanover, 30823 Garbsen, Germany (e-mail: ludger.overmeyer@ita.uni-hannover.de).

Digital Object Identifier 10.1109/JPHOT.2021.3111298

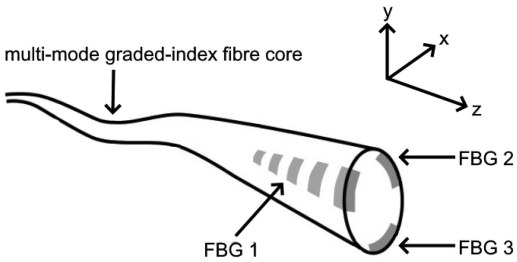

Fig. 1. Schematic concept of the sensor for 3D bend sensing. Three FBGs with different grating constants are written at the same z-position under the surface of the multimode fiber core. A detailed view is given in Fig. 5.

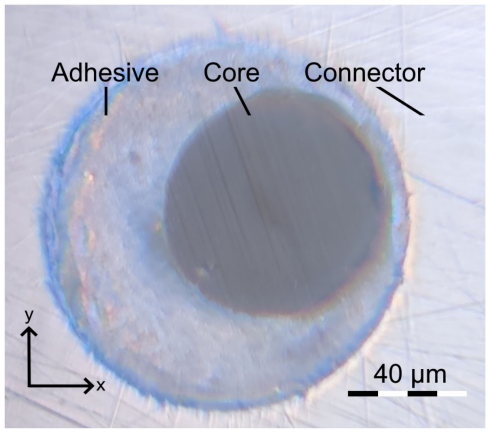

Fig. 2. Microscopic image ($x400$, F1VS400F, Fiber Instrument Sales, Inc.) of a CYTOP fiber-core ($75\ \mu m \pm 10\ \mu m$ diameter, inner circle) glued into an FC/PC-connector with $126\ \mu m$ inner diameter (outer circle). In the middle, the fiber core surrounded by adhesive is visible. Remaining scratches due to grinding can be eliminated by polishing and are not crucial at this point.

II. Materials and Methods

A. Chemical and Mechanical Preparation of POF

In our work, we use graded index Gigapof-50SR multimode polymer fibers (Chromis Fiberoptics) with $50\ \mu m$ core diameter. Initially the coating material of the fiber is chemically removed by placing an approximately $15\ cm$ long part into a cylinder filled with tetrahydrofuran (Carl Roth GmbH + Co. KG). The latter penetrates the coating material and its volume increases, whereas the CYTOP is chemically resistant to the organic solvent. This step is followed by a delamination process and results in a $75\ \mu m \pm 10\ \mu m$ thick bare CYTOP fiber without coating. The remaining core and cladding are then glued into an FC/PC-connector ($126\ \mu m$ inner diameter). Due to the manual process and the viscosity of the glue, the fiber core is usually located off-axis inside the FC/PC-connector. Since light is coupled into the fiber by using a $126\ \mu m$ fiber, sufficient higher order modes are excited and propagate through the sensor section, i.e. the inscribed eccentrical FBGs. Thus, the off-axis position of the fiber inside the connector does not represent a limitation for our work. When the adhesive is cured, the surface of the connector is ground and hand polished with polish film (Fiber Instrument Sales, Inc., $5\ \mu m$; $1\ \mu m$ and $0.3\ \mu m$ grit sizes). The result of this process is controlled by a fiber microscope (F1VS400F, Fiber Instrument Sales, Inc.; Fig. 2). Irregularities of the fiber cross section, as obvious from Fig. 2 are located on the surface only and originate from the polishing process. Generally, they can be minimized by using adhesives with a higher shear strength.

TABLE I
Average Values and Standard Deviations for Measured Sensitivities and Shifts From Fig. 11 (top) and Fig. 12 (bottom), Respectively. Values Are Formed From Five Samples.

Curvature (m^{-1})	Sensitivity (pm/m^{-1})	
	Stretching	Compression
148,15	9,47±4,2	-4,06±2,19
80	12,53±5,43	-6,89±6,89
40	13,78±11,24	-7,53±4,52
26,67	16,91±14,53	-11,29±5,38
20	20,05±8,48	-2,5±13,48
10	25±23,22	-15±24,41

Curvature (m^{-1})	Shift (nm)	
	Stretching	Compression
148,15	1,40±0,62	-0,60±0,32
80	1,00±0,43	-0,55±0,11
40	0,55±0,45	-0,30±0,18
26,67	0,45±0,39	-0,30±0,14
20	0,40±0,17	-0,05±0,27
10	0,25±0,23	0,15±0,24

B. Bragg Grating Inscription

For fabricating of the FBGs the phase mask technique with contact exposure is applied. A pulsed (5-8 ms) KrF Excimer Laser (Atlex FBG-300, ATL Lasertechnik GmbH) generates UV light with $248.3\ nm$ wavelength, which is directed by three mirrors (99.0% reflectance at 45°, Spectral Products) and a cylindrical focus lens onto a phase mask ($\pm 1^{st}$ order optimized, Ibsen Photonics A/S). The grating side of the phase mask is placed directly onto the POF and grating lines are orientated perpendicular to the fiber. The POF itself is fixed by a rotatable connector on one side and a rotatable fiber clamp on the other side. For bend detection the individual FBGs of each triplet are inscribed at fiber rotation angles of 0°/360°, 120° and 240°, to not interact with each other. Phase masks with grating periods of $1065\ nm$, $1070\ nm$, $1080\ nm$, $1100\ nm$ and $1120\ nm$ are utilized for different experiments. Grating periods of $1080\ nm$, $1100\ nm$ and $1120\ nm$ are used to create the FBG triplets, as their reflection signals have sufficient spacing with respect to each other, whereas the grating periods of $1065\ nm$ and $1070\ nm$ are utilized for test measurements. During inscription of the FBG triplets only the corresponding signals were detected and each signal remained stable during the inscription of further FBGs from different angles. Laser pulse parameters of $15\ Hz$ and $6\ mJ$ are employed within two consecutive inscription processes of $256\ s$ each, which are paused by one minute to reduce fiber damage by overheating. The setup is described in detail in [7], [19]. When UV light irradiates the molecular structure of polymers, molecular bonds are broken and the radiation is dissipated. The initial penetration depth of UV light into polymers is only a few μm and increases with the time of illumination, since the number of bonds to break within the initial penetration depth decreases. In this experiment the fiber is located some cm above the focal spot of the cylindrical lens, so the power per area is relatively low to prevent fiber damage due to high radiation. Also this allows for more control over the duration of the inscription process, which significantly depends on the illumination time. The low amount of radiation only structures the polymer on and directly below the cladding and since the illumination time of $2 \times 256\ s$ is relatively short, only eccentrical FBGs are generated

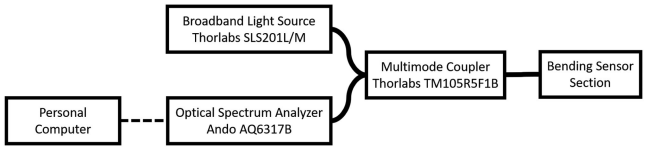

Fig. 3. Measurement setup to detect and evaluate reflected signals from the bend sensor.

in the core, whereas also the center of the multimode fiber core would be modified with a longer exposition to UV radiation.

C. Optical Analysis

Samples are inspected by an optical interrogation system consisting of a broadband light source (Thorlabs SLS201 L/M), a 50:50 Y-coupler (Thorlabs TM105R5F1B) and an optical spectrum analyzer (Ando AQ6317B), which detects Bragg gratings in reflection mode only with a resolution of up to 20 pm (see Fig. 3). Light is coupled into the multimode fiber from the broadband light source, by using the multimode coupler and propagates to the sensor section, which consists of a single fiber with one or multiple FBGs. Reflected signals from the FBGs are split by the multimode coupler and detected by the optical spectrum analyzer and processed on a personal computer. To enhance coupling effects and to suppress refraction, index matching oil ($n = 1.4$, Cargille Laboratories) can be applied on the coupling surfaces between the sensor and the coupler fibers. This method allows scanning of the spectrum while the inscription process is ongoing.

For measuring of the wavelength shift of FBG characteristic spectra during bending, fibers are inserted in 3D printed tools with guide grooves of predefined radii. Fibers are bent downwards and upwards with defined radii of 6.75 mm, 12.5 mm, 25 mm, 37.5 mm, 50 mm, 100 mm, respectively. As reference measurement a "straight" groove is used. Consecutively the reflectivity of the fibers is measured statically in their bending position.

Refractive index values and profiles of the produced samples' cross-sections are measured with an optical index refractometer (RINCK elektronik) with a reference glass ($n = 1.44$) and distilled water ($n = 1.34$) as reference liquid. Confocal microscopy (μscan, NanoFocus AG) is performed to observe the surface of structured fibers (see Fig. 4). After the UV inscription process, densification of the modified material occurs, which alternates with unmodified material, located in the shadow of the grating. This leads to a change of the surface topography as well. Furthermore, bright field microscopy (BA310 LED Trinocular, Motic Deutschland GmbH) is performed with change of the focus to scan through the sample and check if the gratings are located on the surface only or reach deeper inside the fiber cores (Fig. 5). To eliminate temperature cross-sensitivity, all experiments are performed at a temperature of 21.5° C with exception of the refractive index measurement.

III. Results & Discussion

A. Evolution of FBGs During and After Inscription

After starting of the inscription process we observe an immediate generation of a weak intensity peak due to evolution of an FBG, which increases with process time, as long as the laser is switched on. After 6 min the FBG peak reaches the

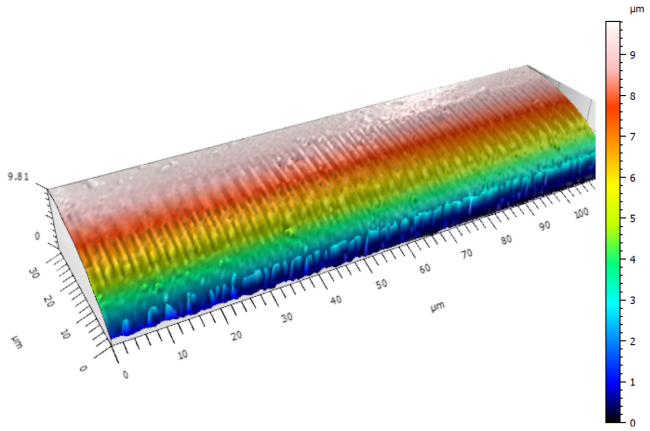

Fig. 4. Confocal microscopic image ($x50$, μscan, NanoFocus AG) of a structured fiber section. The colors indicate the height of the structured area in vertical direction. The grating periods on the surface can be observed in the yellow and red region. The average peak to valley height of the surface grating is 200 nm.

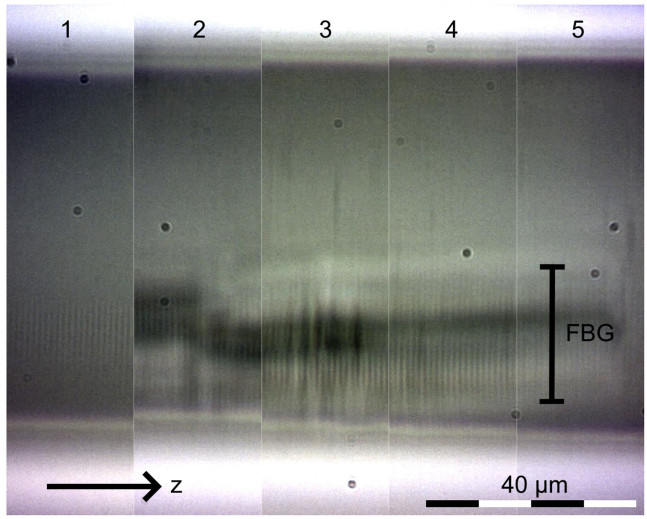

Fig. 5. Transmission microscopic images ($x40$, BA310 LED Trinocular, Motic Deutschland GmbH), as illustrated in Fig. 1, with a single structured section of CYTOP fiber imaged at 5 different focus depths. Depth 1 shows the surface of the fiber, while the depths 2-5 show the FBG structure inside the fiber with increasing focus depths, achieved by shifting the focal distance of the microscope. Black dots originate from dust particles inside the microscope.

same magnitude as after 4 min due to the break of one minute in illumination and it rises again during the second inscription process after the break. During the break of one minute and after the whole inscription process the signal decreases notably but with smaller rate until it equilibrates (Fig. 6). A further decrease of the peak is observed on larger time scales of days and weeks, see below (Fig. 7). The decrease of signal power can be explained by diffusion processes within the material [27], which reduce the refractive index difference between modified and unmodified material over the length of the structured sections as well as the effective area of the grating. This, in turn, affects the propagation of modes, which were interacting with the grating before. Since the grating is inscribed eccentrically mostly lower order propagation modes are affected and do not interact with the grating anymore, which leads to a decrease in the longer wavelength area of the reflected intensity peak, while the lower

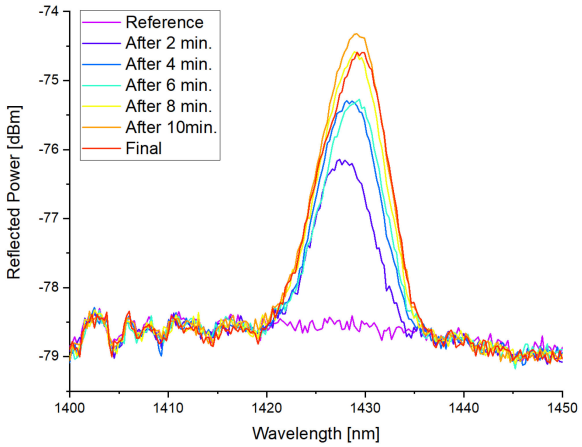

Fig. 6. Increase of the FBG reflection peak as function of time. After switching off the laser, the signal drops quickly (orange, from a maximum of $-74.32\ dBm$) to its final level (red, $-74.59\ dBm$) and the FBG has a maximum reflectivity of $4.02\ dB$ and a full width at half maximum (FWHM) of $8.49\ nm$.

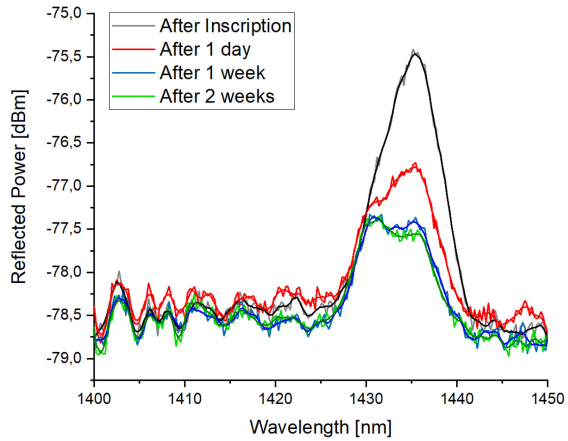

Fig. 7. Decrease of the reflection peak at $1437\ nm$ as a function of time. At $1431\ nm$ a stable reflection peak remains after two weeks with a smaller side peak at $1437\ nm$. The decrease is explained by diffusion processes in the fiber core. The two peaks originate from different propagating mode groups.

wavelength part is relatively stable. After one week the FBG peak wavelength shifts by $6\ nm$ into the blue.

B. Optical Index Refractometry

The effective refractive index of the Bragg gratings can be calculated by $\lambda_{Bragg} = n_{eff} \times 2 \times \Lambda$, with the Bragg wavelength λ_{Bragg} and the grating constant Λ. Assuming that modified (n_{UV}) and unmodified (n_{normal}) sections in FBGs have an even thickness and sharp boundaries the effective refractive index can be calculated with $n_{eff} = (n_{normal} + n_{UV})/2$. The effective refractive index of the inscribed fiber core with $\lambda_{Bragg} \approx 1427\ nm$ and $\Lambda = 1065\ nm/2$ is $n_{eff} \approx 1.3399$, which agrees well with the one given in literature for CYTOP $(n_{Literature} = 1.34)$ [28]. Optical index refractometry measurements show that the values of unmodified fibers lie in a range of $n_{normal} = 1.335 \pm 0.003$, whereas UV-structured fibers have a refractive index of $n_{UV} = 1.342 \pm 0.003$. Calculation confirms the effective refractive index of 1.339. Fig. 8 shows examples of the refractive index profile of unmodified and UV-modified specimen used. The modified fiber has a higher refractive index

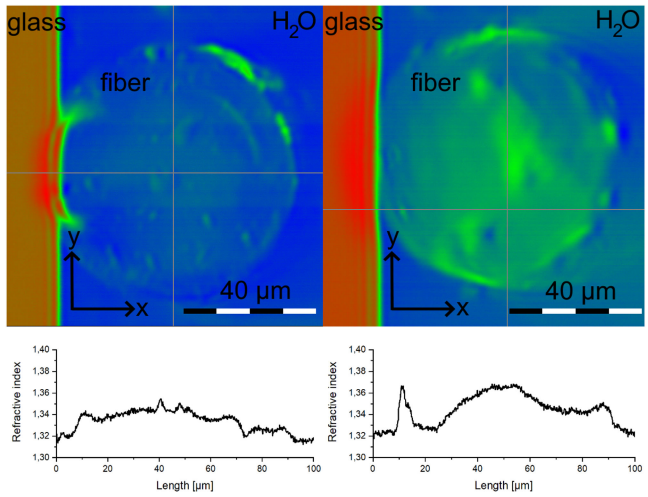

Fig. 8. Top: Area measurement of refractive index using an index refractometer (RINCK elektronik) of an unmodified (left) and a UV-modified (right) fiber with distilled water as surrounding medium and reference glass on the left. Bottom: Refractive index line profiles of the same samples along the y-direction.

on the bottom side, where the modification is located. Fluctuations are due to impurities coming from the polishing process or tensions at the surface. No FBG is inscribed here, since it is necessary to measure the UV-induced change of the material only.

C. Bending Detection and Measurement Sensitivity

When bending is applied, the fibers show a shift of their reflected FBG peak signal. When bending the fiber in a direction in which the grating is stretched or compressed, a red or blue shift appears for the Bragg wavelength, respectively (Fig. 9). It is clearly visible, that gratings, while being in compression mode and therefore located on the inner part of the bent fiber, exhibit a decrease in signal power. On the other hand, gratings in stretching mode being located on the outer bending position exhibit an increase in signal power. This can be explained with the fiber guiding more light in the outer part compared to the inner part of the core. This also enables to detect a bending just by measuring the power in a specific wavelength range. In contrast, previous works with single mode fibers measured a wavelength shift only [1], [2], [5].

In Fig. 10 different selected data curves from Fig. 9 are normalized to highlight the red and blue shifts of the Bragg wavelength increasing with decreasing bend radius and shifting away from the initial reference measurement (straight). The bending sensitivity (Fig. 11) of the produced FBGs is calculated from the shift of the Bragg wavelength $\Delta\lambda_{Bragg}$ depending on the curvature $C = \frac{1}{r}$, with r being the bend radius [2], [5]. Calculations are performed with samples with a single FBG (see Fig. 9). A measured maximum bending sensitivity of $65\ pm/m^{-1}$ could be achieved with a curvature of only $10\ m^{-1}$ (bend radius $100\ mm$) and a wavelength shift of $650\ pm$ in stretching mode. For higher curvatures ($r = 6.75\ mm$) a measured maximum shift of $1950\ pm$ is observed in stretching mode and of $-1450\ pm$ in compression mode with sensitivities of up to $13\ pm/m^{-1}$ and $10\ pm/m^{-1}$, respectively (Fig. 12). The sensor's measured sensitivities decreased to a minimum of $\pm 4\ pm/m^{-1}$ in compression mode $(-)$ and stretching mode

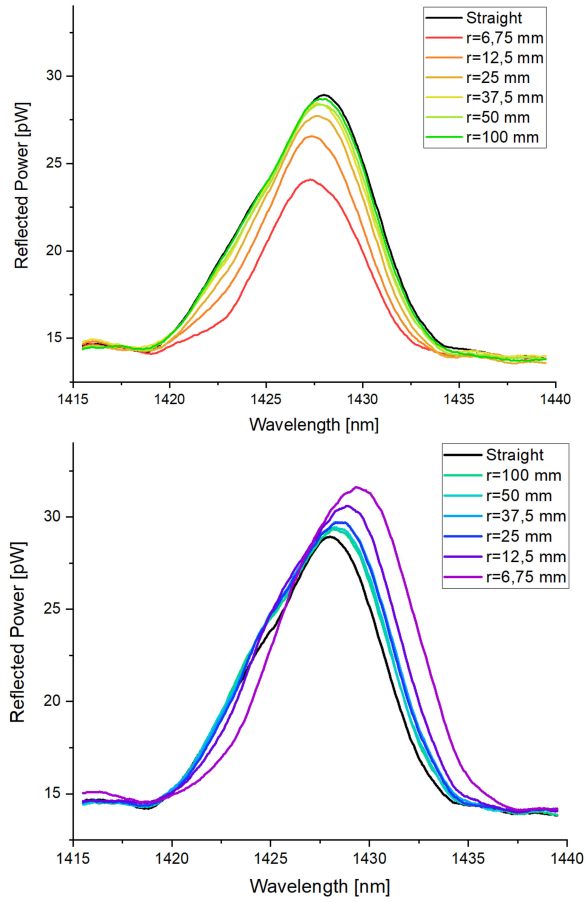

Fig. 9. Reflected FBG peak signal for different bending radii. It is obvious that the peak in maximum compression mode (top) exhibits a decrease in signal power, while in maximum stretching mode (bottom) it exhibits an increase, the magnitude of the two being different due to the different mechanical deformations acting on the grating.

(+) with shifts of $\pm 601\ pm$ at maximum bending, respectively. Although these shifts are currently relatively small, they are reliably detectable at a measurement resolution of $20\ pm$ with state of the art technology. Thus, the approach is suited to quantify bending or shape deformation of surfaces, where the fibers are attached to. Since for larger bending radii the measurement uncertainty is higher compared to the case of smaller radii, we conclude that the current mechanical holder with guide grooves is not ideal for the former, as it does not fixate the fibers sufficiently tight and allows twists in the fiber. An explanation lies in the natural bend shape of the fiber, which originates from the storage on a spool. Due to fiber twist the FBG peak shifts for higher curvatures are varying more obvious than for smaller curvatures, since the former are generally higher and the fiber twist is affecting them stronger. As this is not a fundamental limitation, we expect a significant increase in measurement accuracy and thus sensitivity with an improved fiber holder in place.

Analysis of the azimuthal orientation of the fiber's bending for the smallest bending radius of $6.25\ mm$ in upward direction is performed with increments of 30° rotation of the fiber connector. The FBG is inscribed at an angle of 0°/360°. The measurements show small deviations between the initial measurement at 0° and at the control measurement of 360° approximately 30 minutes later, which derives from the aforementioned loose fixation in the

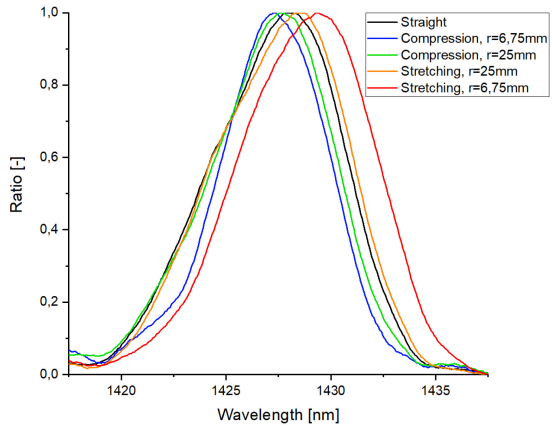

Fig. 10. Normalized reflected FBG peak signal for selected bending radii. The Bragg wavelength undergoes a red or blue shift under stretching or compression of the grating, respectively. The difference between the shift from maximum stretching to maximum compression is $2\ nm$ in this case.

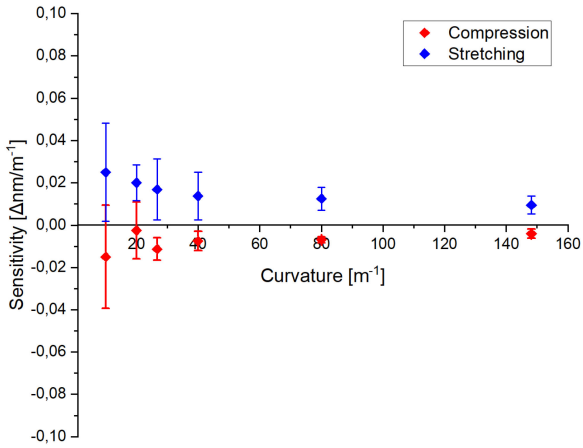

Fig. 11. Average sensitivity of the bend fibers from Fig. 9 as a function of curvature. The highest sensitivity is achieved for larger bending radii. Error bars represent the standard deviation.

mechanical holder. As expected at 180° the maximum reflected signal power and shift are detected reproducibly. In contrast to the expectation, the minimum is not detected at $0/360$ °, but instead of 90°. This is explained by the twist of the fiber, which already applies at 0°/360° to act against the applied bending into upward direction. With further rotation of the fiber more force is applied against the natural twisting behavior. At 90° rotation of the connector, the minimum signal and shift are detected and afterwards the applied force overcomes the natural twisting of the fiber and the signal and shift rises again until an azimuthal angle of 180° is achieved. With further rotation of the connector the signal and the shift of the peak decrease constantly.

D. 3D Bend Detection With Three Gratings

To quantify bending in all three dimensions, FBG triplets are inscribed into the fiber as shown in Fig. 1. A sensitization effect of the fibers is found which leads to nonuniform intensity of the FBG with increasing time of the fiber under the effect of UV light, whereas no interaction between the different FBGs is found in the spectrum. Therefore we conclude, that the gratings do not overlap inside the fiber. In the simplest case, bending is realized with one FBG above the bending plane and two

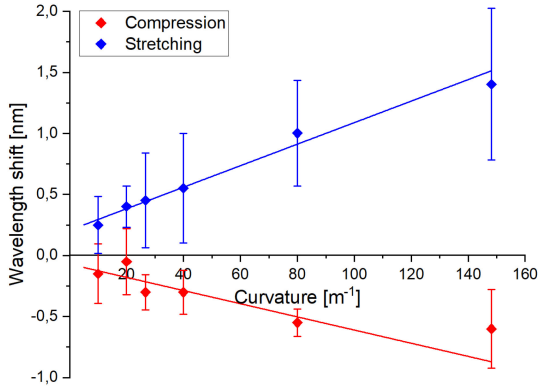

Fig. 12. Average shift of the Bragg wavelength as a function of the fiber curvature based on the results from Fig. 9. The curve fit gives a good approximation for a linear relationship between the wavelength shift and the bend radius or the curvature. Error bars represent the standard deviation.

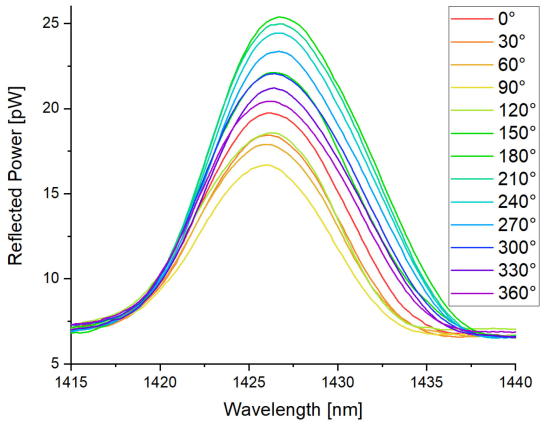

Fig. 13. Average spectrum of reflected power with fibers in $6.25\ mm$ upward bending direction at different azimuthal orientations. As expected at 180° the maximum is observed, whereas in contrast the minimum is observed at 90° instead of the expected 0°/360°.

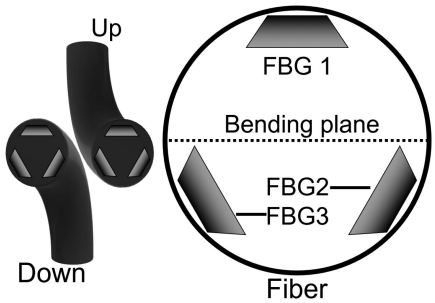

Fig. 14. The three-dimensional bending situation, when the fiber is bent up and down, as well as the positions of the three FBGs inside the fiber core with respect to the bending plane.

FBGs below (Fig. 14) with the fiber bending in previously mentioned radii and directions. However, when only one FBG is located on each side of the bending plane and the third FBG is exactly in the bending plane, bend detection is still possible. Here it has to be pointed out, that writing of additional FBGs in one section is not interfering with already existing FBGs due to the rotation of the fiber and the size of each grating area. When the fiber is bent upwards (downwards), the grating above the bending plane undergoes compression (stretching), whereas

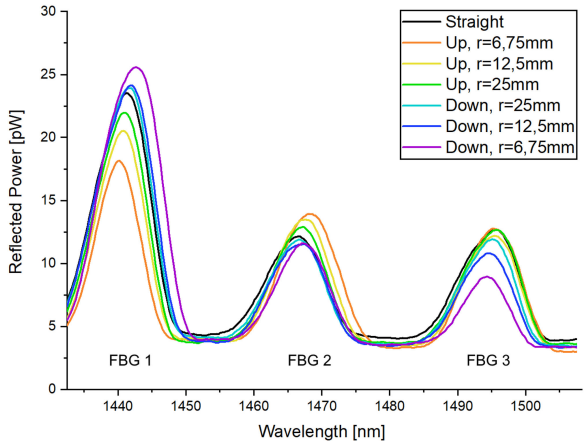

Fig. 15. Reflectivity of an FBG triplet for selected bending radii. The Bragg wavelengths undergo an increase or decrease of signal power as well as a red or blue shift under stretching or compression of the grating positions inside the core.

the gratings below the bending plane undergo the opposite. In Fig. 15, FBG 1 shows the expected behavior with regard to bending as shown in Fig. 9. FBGs 2 and 3 show an opposite effect, which indicates that both are located on the other side of the bending plane. In addition, for the smallest bending radii of $6,25\ mm$ in downward bending direction FBGs 2 and 3 show opposite wavelength shifts. The observed variation in FBG peak shifts for identical bending cases and radii applied can be attributed to small twists of the fibers induced by the mechanical fixation during the measurements (Fig. 13). When the fiber is bent upwards, it is twisted with rotation in clockwise direction (see Fig. 14). FBG 1 is moved towards the bending plane but is still further away from it. FBG 2 is moved away from the bending plane, which leads to a stronger change in the signal. Finally, FBG 3 is moved towards the bending plane as well, but in contrast to FBG 1 it is closer to it. Consequently, FBG 1 exhibits less sensitivity to bending. The reaction of FBG 2 is improved compared to the theoretical model, whereas FBG 3 is showing only slight differences compared to the straight reference measurement. When the fiber is bent downwards, it is twisted by rotating counterclockwise, thus, the signals of FBGs 2 and 3 are changed now. However, this is not decisive for the proof-of-principle experiment. The peak power of FBG 1 is stronger, which can have multiple causes such as different strain on the fiber due the inscription process, however, the peak power itself is not the main relevant parameter. Instead, the individual behaviour of each peak under bending needs to be considered. Depending on the individual effect on each grating to bending the bending direction can be calculated, if the exact positions of the gratings inside the fiber are known. If the latter are unknown, but the directions of the first two bend movements are known, the grating positions can be calculated in turn. If the exact positions of the three FBGs are not known, as is the case in applications, for example, it is possible to perform reference measurements, in which the ultimate bending positions are determined. With one reference in a straight fiber position and one reference in a known direction, a third measurement's direction and bending radius can be calculated from the detected spectrum of the three gratings. Also the exact positions of the three FBGs can be determined with these reference measurements as long as there is no fiber twist in the reference bending measurement.

IV. Conclusion

In summary, we demonstrated a new and simple sensor to detect and characterize bending with high sensitivity based on eccentric FBGs in POF. The sensor is capable to measure one-directional bending with a sensitivity of $30\ pm/m^{-1}$, which is higher compared to previous works (see e.g. [5]), where, in addition, mostly multi-core and single mode fibers were used. For the smallest bending radii applied, wavelength shifts of up to $1.3\ nm$ in stretching mode and sensitivities as low as $9\ pm/m^{-1}$ are reproducibly observed. Furthermore, it is possible to use only the peak signal of the individual FBGs for bend monitoring to realise a simplified sensor with LEDs as light sources and a powermeter for measurement. In addition it is worth noting, that the sensor is capable of reliably measuring at small bend radii, at which common glass fibers fail to guide light or even break. Due to phase mask technique employed and the multimode fiber used, the technique is very cost-efficient.

Our setup also enables to write multiple FBGs with different grating constants at one position of a multimode fiber along the optical axis. This offers the possibility to quantify bending in all three dimensions. The developed technology represents a promising approach for applications in medical diagnostics to detect motion of patients [29]–[31], in robotics and augmented reality scenarios including gaming gloves or in motion-recording wearables for use in sports and motion capture [32], [33], to name a few.

Disclosures

The authors declare no conflicts of interest.

References

[1] A. Martinez, Y. Lai, M. Dubov, I. Y. Khrushchev, and I. Bennion, "Vector bending sensors based on fibre Bragg gratings inscribed by infrared femtosecond laser," *Electron. Lett.*, vol. 41, no. 8, pp. 472–474, 2005.

[2] X. Chen, C. Zhang, D. J. Webb, K. Kalli, and G.-D. Peng, "Highly sensitive bend sensor based on Bragg grating in eccentric core polymer fiber," *IEEE Photon. Technol. Lett.*, vol. 22, no. 11, pp. 850–852, Jun. 2010.

[3] Y. Luo *et al.*, "Analysis of multimode POF gratings in stress and strain sensing applications," *Opt. Fiber Technol.*, vol. 17, no. 3, pp. 201–209, 2011.

[4] K. Bremer, T. Reinsch, G. Leen, B. Roth, S. Lochmann, and E. Lewis, "Pressure, temperature and refractive index determination of fluids using a single fibre optic point sensor," *Sensors Actuators A: Phys.*, vol. 256, pp. 84–88, 2017.

[5] X. Hu, X. Chen, C. Liu, P. Mégret, and C. Caucheteur, "D-shaped polymer optical fiber Bragg grating for bend sensing," in *Proc. Adv. Photon.*, 2015, paper SeS2B.5.

[6] T. Li, C. Shi, Y. Tan, R. Li, Z. Zhou, and H. Ren, "A diaphragm type fiber Bragg grating vibration sensor based on transverse property of optical fiber with temperature compensation," *IEEE Sensors J.*, vol. 17, no. 4, pp. 1021–1029, Feb. 2017.

[7] Y. Zheng, K. Bremer, and B. Roth, "Investigating the strain, temperature and humidity sensitivity of a multimode graded-index perfluorinated polymer optical fiber with Bragg grating," *Sensors*, vol. 18, no. 5, 2018, Art. no. 1436.

[8] K. Peters, "Polymer optical fiber sensors — A review," *Smart Mater. Struct.*, vol. 20, 2011, Art. no. 013002.

[9] Z. Xiong, G. D. Peng, B. Wu, and P. L. Chu, "Highly tunable Bragg gratings in single-mode polymer optical fibers," *IEEE Photon. Technol. Lett.*, vol. 11, no. 3, pp. 352–354, Mar. 1999.

[10] I. Johnson, D. Webb, K. Kalli, M. C. Large, and A. Argyros, "Multiplexed FBG sensor recorded in multimode microstructured polymer optical fibre," in *Proc. Photonic Cryst. Fivers IV*, vol. 7714, 2010, Art. no. 77140D.

[11] R. Min *et al.*, "Inscription of Bragg gratings in undoped PMMA mPOF with ND:YAG laser at 266 nm wavelength," *Opt. Exp.*, vol. 27, no. 26, pp. 38039–38048, 2019.

[12] L. M. Pereira *et al.*, "Phase-shifted Bragg grating inscription in PMMA microstructured POF using 248 nm UV radiation," *J. Lightw. Technol.*, vol. 35, no. 23, pp. 5176–5184, 2017.

[13] R. Min, B. Ortega, A. Leal-Junior, and C. Marques, "Fabrication and characterization of Bragg grating in CYTOP POF at 600 nm wavelength," *IEEE Sens. Lett.*, vol. 2, no. 3, pp. 1–4, Sep. 2018.

[14] A. Lacraz, M. Polis, A. Theodosiou, C. Koutsides, and K. Kalli, "Femtosecond laser inscribed Bragg gratings in low loss CYTOP polymer optical fiber," *IEEE Photon. Technol. Lett.*, vol. 27, no. 7, pp. 693–696, Apr. 2015.

[15] J. Meyer, A. Nedjalkov, C. Kelb, G. J. Strobel, L. Ganzer, and W. Schade, "Manufacturing and characterization of femtosecond laser-inscribed Bragg grating in polymer waveguide operation in an IR-A wavelength range," *Sensors*, vol. 20, no. 1, 2020, Art. no. 249.

[16] A. Theodosiou, K. Kalli, A. Gillooly, and A. Ioannou, "Carbon coated FBGs inscribed using the plane-by-plane femtosecond laser inscription method," in *Proc. 7th Eur. Workshop Opt. Fibre Sensors*, vol. 11199, 2019, Art. no. 111992Z.

[17] A. Theodosiou *et al.*, "Er/yb double-clad fiber laser with fs-laser inscribed plane-by-plane chirped FBG laser mirrors," *IEEE Photon. Technol. Lett.*, vol. 31, no. 5, pp. 409–412, Mar. 2019.

[18] M. Koerdt *et al.*, "Fabrication and characterization of Bragg gratings in perfluorinated polymer optical fibers and their embedding in composites," *Mechatronics*, vol. 34, pp. 137–146, 2016.

[19] K. Bremer, F. Weigand, Y. Zheng, L. S. Alwis, R. Helbig, and B. Roth, "Structural health monitoring using textile reinforcement structures with integrated optical fiber sensors," *Sensors*, vol. 17, no. 2, 2017, Art. no. 345.

[20] D. Sartiano, S. Sales, and E. T. Roca, "Three lobes plastic optical fiber bending and rotation sensor," in *Multidisciplinary Digit. Publishing Inst. Proc.*, vol. 15, no. 1, p. 1–5, Jul. 2019.

[21] A. Ghaffar *et al.*, "Twisted macro-bend coupling based three-dimensional displacement measurement sensor using polymer fiber," *OSA Continuum*, vol. 2, no. 9, pp. 2773–2782, 2019.

[22] H. Zhang *et al.*, "Fiber Bragg gratings in heterogeneous multicore fiber for directional bending sensing," *J. Opt.*, vol. 18, no. 8, 2016, Art. no. 085705.

[23] K. Yang *et al.*, "Femtosecond laser inscription of fiber Bragg grating in twin-core few-mode fiber for directional bend sensing," *J. Lightw. Technol.*, vol. 35, no. 21, pp. 4670–4676, 2017.

[24] F. Khan, A. Denasi, D. Barrera, J. Madrigal, S. Sales, and S. Misra, "Multi-core optical fibers with Bragg gratings as shape sensor for flexible medical instruments," *IEEE Sensors J.*, vol. 19, no. 14, pp. 5878–5884, Jul. 2019.

[25] W. Bao *et al.*, "Selective fiber Bragg grating inscription in four-core fiber for two-dimension vector bending sensing," *Opt. Exp.*, vol. 28, no. 18, pp. 26 461–26469, 2020.

[26] A. G. Leal-Junior *et al.*, "FPI-POFBG angular movement sensor inscribed in CYTOP fibers with dynamic angle compensator," *IEEE Sensors J.*, vol. 20, no. 11, pp. 5962–5969, Jun. 2020.

[27] A. Baum, P. J. Scully, W. Perrie, D. Liu, and V. Lucarini, "Mechanisms of femtosecond laser-induced refractive index modification of PMMA," *J. Opt. Soc. Amer.*, vol. 27, no. 1, pp. 107–111, 2010.

[28] T. Ishigure, Y. Koike, and J. W. Fleming, "Optimum index profile of the perfluorinated polymer-based GI polymer optical fiber and its dispersion properties," *J. Lightw. Technol.*, vol. 18, no. 2, pp. 178–184, 2000.

[29] L. Leffers, J. Locmelis, K. Bremer, B. Roth, and L. Overmeyer, "Eccentrical Bragg gratings in multimode polymer optical fibres for the 3D detection of bending," in *Micro-Structured Specialty Opt. Fibres VII*, 2021, vol. 11773, Art. no. 117730R.

[30] M. F. Domingues *et al.*, "Insole optical fiber Bragg grating sensors network for dynamic vertical force monitoring," *J. Biomed. Opt.*, vol. 22, no. 9, 2017, Art. no. 91507.

[31] V. Mishra, N. Singh, U. Tiwari, and P. Kapur, "Fiber grating sensors in medicine current and emerging applications," *Sensors Actuators A*, vol. 167, pp. 279–290, 2011.

[32] L. Overmeyer, F. Podszus, and L. Dohrmann, "Multimodal speech and gesture control of AGVs, including EEG-based measurements of cognitive workload," *CIRP Ann. - Manuf. Technol.*, vol. 65, no. 1, pp. 425–428, 2016.

[33] S. Sundaram, P. Kellnhofer, Y. Li, J.-Y. Zhu, A. Torralba, and W. Matusik, "Learning the signatures of the human grasp using a scalable tactile glove," *Nature*, vol. 569, no. 7758, pp. 698–702, 2019.